The effects of spatial relations and motion information in social scene perception - Supplementary material

Violette Munin, Etienne Abassi, Pierre-Aurélien Beuriat, Liuba Papeo

Supplementary material 1

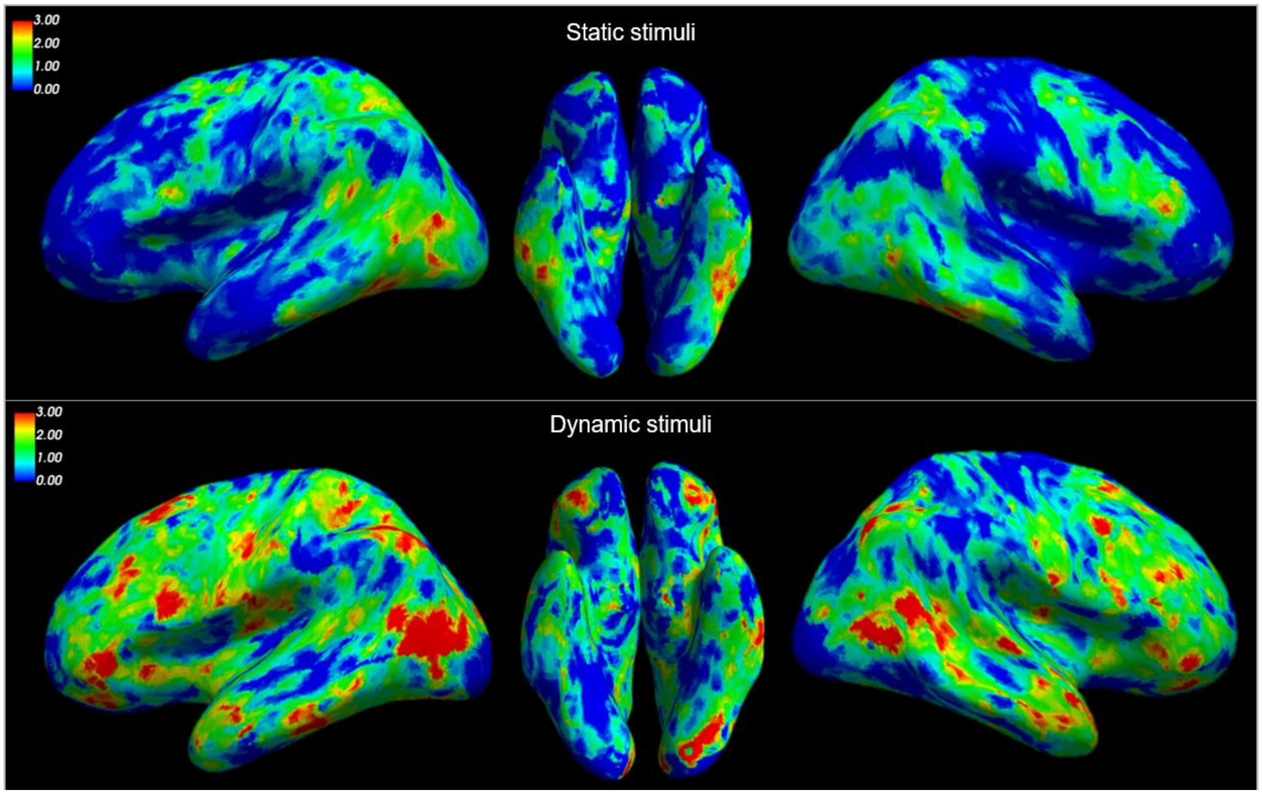

Figure S1. Unthresholded statistical maps for the contrasts facing > nonfacing with static (upper row) and dynamic (lower row) stimuli.

Supplementary material 2

Table S1. MNI coordinates for the 15 participants of functionally localized EBA and pSTS, and of facing > non-facing activity peaks for static and dynamic sets.

EBA						pSTS						Facing > Non-facing peak					
Left			Right			Left			Right			Static			Dynamic		
x	y	z	x	y	z	x	y	z	x	y	z	x	y	z	x	y	z
-51	-78	-1	52	-78	3	-59	-47	25	59	-43	16	33	-58	3	**-46**	**-80**	**16**
-53	*-82*	*7*	*50*	*-73*	*5*	-61	-43	25	63	-38	21	**-57**	**-73**	**10**	**-57**	**-67**	**12**
-53	-73	7	54	-71	3	-51	-45	29	59	-38	14	**-53**	**-78**	**14**	**-44**	**-69**	**7**
-51	-76	10	48	-78	12	-55	-47	25	68	-36	21	52	-67	16	**-51**	**-76**	**1**
-48	-76	1	46	-67	1	-51	-49	12	61	-49	25	33	-47	12	33	-62	21
-42	-76	-1	46	-71	-10	*-57*	*-65*	*14*	*44*	*-58*	*7*	**-57**	**-89**	**16**	57	-45	1
-48	-73	14	48	-80	7	-68	-41	25	57	-43	21	**-51**	**-73**	**12**	**-55**	**-67**	**12**
-57	-76	16	54	-76	7	*-57*	*-65*	*14*	*44*	*-58*	*7*	63	-87	3	**-42**	**-82**	**-4**
-51	-73	12	57	-71	7	-57	-23	27	52	-54	10	46	-71	-12	**-55**	**-65**	**27**
-51	-76	14	50	-69	14	-64	-56	29	59	-54	12	**-59**	**-58**	**32**	50	-91	12
-48	-82	3	57	-65	-1	-64	-38	25	61	-34	18	**-68**	**-67**	**21**	**-48**	**-49**	**12**
-57	-76	10	54	-73	7	*-57*	*-65*	*14*	*44*	*-58*	*7*	**-64**	**-62**	**-4**	**-57**	**-67**	**16**
-48	-80	3	44	-71	-8	-68	-54	32	50	-54	10	**-55**	**-69**	**12**	**-46**	**-82**	**3**
-46	-89	10	50	-82	-6	-70	-32	25	68	-30	23	**-59**	**-69**	**10**	**-66**	**-76**	**-6**
-42	-62	-4	48	-73	-8	-66	-41	23	65	-62	-6	41	-69	3	**-44**	**-76**	**21**

Notes: coordinates of static and dynamic peaks located in the left hemisphere are in bold. Italics are group level coordinates used when no active voxels were found.

Supplementary material 3

Table S2: Mean number of voxels in each ROI across participants before and after removing overlapping voxels between ROIs.

		Left		Right	
		Before	*After*	*Before*	*After*
EBA	Mean	100	95.1	100	83.9
	SD	0	5.2	0	16.4
MTV5	Mean	91.9	87.3	92.9	72.4
	SD	24.6	24.8	19.2	22.1
pSTS	Mean	98.8	98.5	92.9	87.3
	SD	3.2	3.1	18.6	18.4
PPA	Mean	100	100	100	100
	SD	0	0	0	0
EVC	Mean	100	100	100	100
	SD	0	0	0	0

Supplementary material 4

fMRIPrep preprocessing steps

Preprocessing of B_0 inhomogeneity mappings

One fieldmap was used for each subject. A B_0 nonuniformity map (or fieldmap) was estimated from the phase-drift map(s) measure with two consecutive GRE (gradient-recalled echo) acquisitions. The corresponding phase-map(s) were phase-unwrapped with prelude (FSL 6.0.5.1:57b01774).

Anatomical data preprocessing

One T1-weighted (T1w) images was used within each dataset. The T1-weighted (T1w) image was corrected for intensity non-uniformity (INU) with N4BiasFieldCorrection (Tustison et al. 2010), distributed with ANTs 2.3.3 (Avants et al. 2008, RRID:SCR_004757), and used as T1w-reference throughout the workflow. The T1w-reference was then skull-stripped with a Nipype implementation of the antsBrainExtraction.sh workflow (from ANTs), using OASIS30ANTs as target template. Brain tissue segmentation of cerebrospinal fluid (CSF), white-matter (WM) and gray-matter (GM) was performed on the brain-extracted T1w using fast (FSL 6.0.5.1:57b01774, RRID:SCR_002823, Zhang, Brady, and Smith 2001). Brain surfaces were reconstructed using recon-all (FreeSurfer 7.2.0, RRID:SCR_001847, Dale, Fischl, and Sereno 1999), and the brain mask estimated previously was refined with a custom variation of the method to reconcile ANTs-derived and FreeSurfer-derived segmentations of the cortical gray-matter of Mindboggle (RRID:SCR_002438, Klein et al. 2017). Volume-based spatial normalization to two standard spaces (MNI152NLin2009cAsym, MNI152NLin6Asym) was performed through nonlinear registration with antsRegistration (ANTs 2.3.3), using brain-extracted versions of both T1w reference and the T1w template. The following templates were selected for spatial normalization: ICBM 152 Nonlinear Asymmetrical template version 2009c [Fonov et al. (2009), RRID:SCR_008796; TemplateFlow ID: MNI152NLin2009cAsym], FSL's MNI ICBM 152 non-linear 6th Generation Asymmetric Average Brain Stereotaxic Registration Model [Evans et al. (2012), RRID:SCR_002823; TemplateFlow ID: MNI152NLin6Asym].

Functional data preprocessing

For each of the BOLD runs found per subject (across all tasks and sessions), the following preprocessing was performed. First, a reference volume and its skull-stripped version were generated using a custom methodology of fMRIPrep. Head-motion parameters with respect to the BOLD reference (transformation matrices, and six corresponding rotation and translation parameters) are estimated before any spatiotemporal filtering using mcflirt (FSL 6.0.5.1:57b01774, Jenkinson et al. 2002). BOLD runs were slice-time corrected to 0.955s (0.5 of slice acquisition range 0s-1.91s) using 3dTshift from AFNI (Cox and Hyde 1997, RRID:SCR_005927). The BOLD time-series (including slice-timing correction when applied) were resampled onto their original, native space by applying the transforms to correct for head-motion. These resampled BOLD time-series will be referred to as preprocessed BOLD in original space, or just preprocessed BOLD. The BOLD reference was then co-registered to the T1w reference using bbregister (FreeSurfer) which implements boundary-based registration (Greve and Fischl 2009). Co-registration was configured with six degrees of freedom. Several confounding time-series were calculated based on the preprocessed BOLD: framewise displacement (FD), DVARS and three region-wise global signals. FD was computed using two formulations following Power (absolute sum of relative motions, Power et al. (2014)) and Jenkinson (relative root mean square displacement between affines, Jenkinson et al. (2002)). FD and DVARS are calculated for each functional run, both using their implementations in Nipype (following the definitions by Power et al. 2014). The three global signals are extracted within the CSF, the WM, and the whole-brain masks. Additionally, a set of physiological regressors were extracted to allow for component-based noise correction (CompCor, Behzadi et al. 2007). Principal components are estimated after high-pass filtering the preprocessed BOLD time-series (using a discrete cosine filter with 128s cut-off) for the two CompCor variants: temporal (tCompCor) and anatomical (aCompCor). tCompCor components are then calculated from the top 2% variable voxels within the brain mask. For aCompCor, three probabilistic masks (CSF, WM and combined CSF+WM) are generated in anatomical space. The implementation differs from that of Behzadi et al. in that instead of eroding the masks by 2 pixels on BOLD space, a mask of pixels that likely contain a volume fraction of GM is subtracted from the aCompCor masks. This mask is obtained by dilating a GM mask extracted from the FreeSurfer's aseg segmentation, and it ensures components are not extracted from voxels containing a minimal fraction of GM. Finally, these masks are resampled into BOLD space and binarized by thresholding at 0.99 (as in the original implementation). Components are also calculated separately within the WM and CSF masks. For each CompCor decomposition, the k components with the largest singular values are retained, such that the retained components' time series are sufficient to explain 50 percent of variance across the nuisance mask (CSF, WM, combined, or temporal). The remaining components are dropped from consideration. The head-motion estimates calculated in the correction step were also placed within the corresponding confounds file. The confound time series derived from head motion estimates and global signals were expanded with the inclusion of temporal derivatives and quadratic terms for each (Satterthwaite et al. 2013). Frames that exceeded a threshold of 0.5 mm FD or 1.5 standardized DVARS were annotated as motion outliers. Additional nuisance timeseries are calculated by means of principal components analysis of the signal found within a thin band (crown) of voxels around the edge of the brain, as proposed by (Patriat, Reynolds, and Birn 2017). The BOLD time-series were resampled into standard space, generating a preprocessed BOLD run in MNI152NLin2009cAsym space. First, a reference volume and its skull-stripped version were generated using a custom methodology of fMRIPrep. Automatic removal of motion artifacts using independent component analysis (ICA-AROMA, Pruim et al. 2015) was performed on the preprocessed BOLD on MNI space time-series after removal of non-steady state volumes and spatial smoothing with an isotropic, Gaussian kernel of 6mm FWHM (full-width half-maximum). Corresponding "non-aggresively" denoised runs were produced after such smoothing. Additionally, the "aggressive" noise-regressors were collected and placed in the corresponding confounds file. All resamplings can be performed with a single interpolation step by composing all the pertinent transformations (i.e. head-motion transform matrices, susceptibility distortion correction when available, and co-registrations to anatomical and output spaces). Gridded (volumetric) resamplings were performed using antsApplyTransforms (ANTs), configured with Lanczos interpolation to minimize the smoothing effects of other kernels (Lanczos 1964). Non-gridded (surface) resamplings were performed using mri_vol2surf (FreeSurfer).

fMRIPrep bibliography

Abraham, Alexandre, Fabian Pedregosa, Michael Eickenberg, Philippe Gervais, Andreas Mueller, Jean Kossaifi, Alexandre Gramfort, Bertrand Thirion, and Gael Varoquaux. 2014. "Machine Learning for Neuroimaging with Scikit-Learn." Frontiers in Neuroinformatics 8. https://doi.org/10.3389/fninf.2014.00014.

Avants, B. B., C. L. Epstein, M. Grossman, and J. C. Gee. 2008. "Symmetric Diffeomorphic Image Registration with Cross-Correlation: Evaluating Automated Labeling of Elderly and Neurodegenerative Brain." Medical Image Analysis 12 (1): 26–41. https://doi.org/10.1016/j.media.2007.06.004.

Behzadi, Yashar, Khaled Restom, Joy Liau, and Thomas T. Liu. 2007. "A Component Based Noise Correction Method (CompCor) for BOLD and Perfusion Based fMRI." NeuroImage 37 (1): 90–101. https://doi.org/10.1016/j.neuroimage.2007.04.042.

Cox, Robert W., and James S. Hyde. 1997. "Software Tools for Analysis and Visualization of fMRI Data." NMR in Biomedicine 10 (4-5): 171–78. https://doi.org/10.1002/(SICI)1099-1492(199706/08)10:4/5<171::AID-NBM453>3.0.CO;2-L.

Dale, Anders M., Bruce Fischl, and Martin I. Sereno. 1999. "Cortical Surface-Based Analysis: I. Segmentation and Surface Reconstruction." NeuroImage 9 (2): 179–94. https://doi.org/10.1006/nimg.1998.0395.

Esteban, Oscar, Ross Blair, Christopher J. Markiewicz, Shoshana L. Berleant, Craig Moodie, Feilong Ma, Ayse Ilkay Isik, et al. 2018. "fMRIPrep 22.0.2." Software. https://doi.org/10.5281/zenodo.852659.

Esteban, Oscar, Christopher Markiewicz, Ross W Blair, Craig Moodie, Ayse Ilkay Isik, Asier Erramuzpe Aliaga, James Kent, et al. 2018. "fMRIPrep: A Robust Preprocessing Pipeline for Functional MRI." Nature Methods. https://doi.org/10.1038/s41592-018-0235-4.

Evans, AC, AL Janke, DL Collins, and S Baillet. 2012. "Brain Templates and Atlases." NeuroImage 62 (2): 911–22. https://doi.org/10.1016/j.neuroimage.2012.01.024.

Fonov, VS, AC Evans, RC McKinstry, CR Almli, and DL Collins. 2009. “Unbiased Nonlinear Average Age-Appropriate Brain Templates from Birth to Adulthood.” NeuroImage 47, Supplement 1: S102. https://doi.org/10.1016/S1053-8119(09)70884-5.

Gorgolewski, K., C. D. Burns, C. Madison, D. Clark, Y. O. Halchenko, M. L. Waskom, and S. Ghosh. 2011. “Nipype: A Flexible, Lightweight and Extensible Neuroimaging Data Processing Framework in Python.” Frontiers in Neuroinformatics 5: 13. https://doi.org/10.3389/fninf.2011.00013.

Gorgolewski, Krzysztof J., Oscar Esteban, Christopher J. Markiewicz, Erik Ziegler, David Gage Ellis, Michael Philipp Notter, Dorota Jarecka, et al. 2018. “Nipype.” Software. https://doi.org/10.5281/zenodo.596855.

Greve, Douglas N, and Bruce Fischl. 2009. “Accurate and Robust Brain Image Alignment Using Boundary-Based Registration.” NeuroImage 48 (1): 63–72. https://doi.org/10.1016/j.neuroimage.2009.06.060.

Jenkinson, Mark, Peter Bannister, Michael Brady, and Stephen Smith. 2002. “Improved Optimization for the Robust and Accurate Linear Registration and Motion Correction of Brain Images.” NeuroImage 17 (2): 825–41. https://doi.org/10.1006/nimg.2002.1132.

Klein, Arno, Satrajit S. Ghosh, Forrest S. Bao, Joachim Giard, Yrjö Häme, Eliezer Stavsky, Noah Lee, et al. 2017. “Mindboggling Morphometry of Human Brains.” PLOS Computational Biology 13 (2): e1005350. https://doi.org/10.1371/journal.pcbi.1005350.

Lanczos, C. 1964. “Evaluation of Noisy Data.” Journal of the Society for Industrial and Applied Mathematics Series B Numerical Analysis 1 (1): 76–85. https://doi.org/10.1137/0701007.

Patriat, Rémi, Richard C. Reynolds, and Rasmus M. Birn. 2017. “An Improved Model of Motion-Related Signal Changes in fMRI.” NeuroImage 144, Part A (January): 74–82. https://doi.org/10.1016/j.neuroimage.2016.08.051.

Power, Jonathan D., Anish Mitra, Timothy O. Laumann, Abraham Z. Snyder, Bradley L. Schlaggar, and Steven E. Petersen. 2014. “Methods to Detect, Characterize, and Remove Motion Artifact in Resting State fMRI.” NeuroImage 84 (Supplement C): 320–41. https://doi.org/10.1016/j.neuroimage.2013.08.048.

Pruim, Raimon H. R., Maarten Mennes, Daan van Rooij, Alberto Llera, Jan K. Buitelaar, and Christian F. Beckmann. 2015. “ICA-AROMA: A Robust ICA-Based Strategy for

Removing Motion Artifacts from fMRI Data." NeuroImage 112 (Supplement C): 267–77. https://doi.org/10.1016/j.neuroimage.2015.02.064.

Satterthwaite, Theodore D., Mark A. Elliott, Raphael T. Gerraty, Kosha Ruparel, James Loughead, Monica E. Calkins, Simon B. Eickhoff, et al. 2013. "An improved framework for confound regression and filtering for control of motion artifact in the preprocessing of resting-state functional connectivity data." NeuroImage 64 (1): 240–56. https://doi.org/10.1016/j.neuroimage.2012.08.052.

Tustison, N. J., B. B. Avants, P. A. Cook, Y. Zheng, A. Egan, P. A. Yushkevich, and J. C. Gee. 2010. "N4itk: Improved N3 Bias Correction." IEEE Transactions on Medical Imaging 29 (6): 1310–20. https://doi.org/10.1109/TMI.2010.2046908.

Zhang, Y., M. Brady, and S. Smith. 2001. "Segmentation of Brain MR Images Through a Hidden Markov Random Field Model and the Expectation-Maximization Algorithm." IEEE Transactions on Medical Imaging 20 (1): 45–57. https://doi.org/10.1109/42.906424.